JACS
JOURNAL OF THE AMERICAN CHEMICAL SOCIETY

Article

pubs.acs.org/JACS

Chromatin Unfolding by Epigenetic Modifications Explained by Dramatic Impairment of Internucleosome Interactions: A Multiscale Computational Study

Rosana Collepardo-Guevara,[†,‡,#] Guillem Portella,[†,‡,#] Michele Vendruscolo,[†] Daan Frenkel,[†] Tamar Schlick,[*,§,∥] and Modesto Orozco[*,‡,⊥]

[†]Chemistry Department, University of Cambridge, Lensfield Road, Cambridge, CB2 1EW United Kingdom

[‡]Joint BSC-CRG-IRB Programme on Computational Biology, Institute for Research in Biomedicine, Baldiri i Reixac 19, 08028, Barcelona, Spain

[§]Department of Chemistry, New York University, 100 Washington Square East, New York, New York 10003, United States

[∥]Courant Institute of Mathematical Sciences, New York University, 251 Mercer Street, New York, New York 10012, United States

[⊥]Departament de Bioquímica i Biologia Molecular, Facultat de Biologia, Universitat de Barcelona, Avgda Diagonal 643, 08028, Barcelona, Spain

Supporting Information

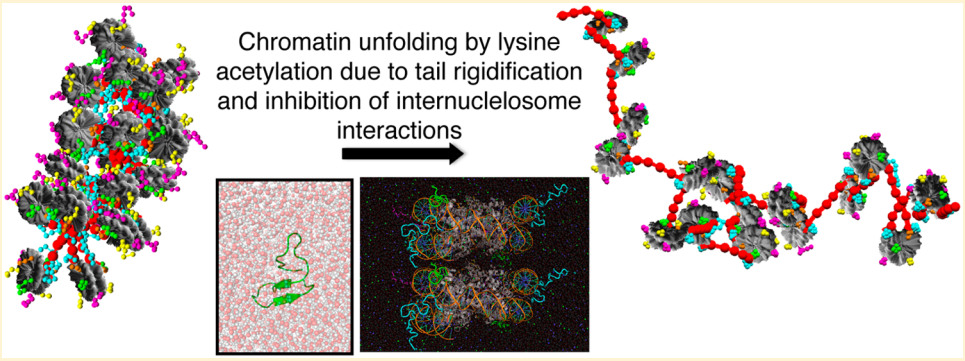

ABSTRACT: Histone tails and their epigenetic modifications play crucial roles in gene expression regulation by altering the architecture of chromatin. However, the structural mechanisms by which histone tails influence the interconversion between active and inactive chromatin remain unknown. Given the technical challenges in obtaining detailed experimental characterizations of the structure of chromatin, multiscale computations offer a promising alternative to model the effect of histone tails on chromatin folding. Here we combine multimicrosecond atomistic molecular dynamics simulations of dinucleosomes and histone tails in explicit solvent and ions, performed with three different state-of-the-art force fields and validated by experimental NMR measurements, with coarse-grained Monte Carlo simulations of 24-nucleosome arrays to describe the conformational landscape of histone tails, their roles in chromatin compaction, and the impact of lysine acetylation, a widespread epigenetic change, on both. We find that while the wild-type tails are highly flexible and disordered, the dramatic increase of secondary-structure order by lysine acetylation unfolds chromatin by decreasing tail availability for crucial fiber-compacting internucleosome interactions. This molecular level description of the effect of histone tails and their charge modifications on chromatin folding explains the sequence sensitivity and underscores the delicate connection between local and global structural and functional effects. Our approach also opens new avenues for multiscale processes of biomolecular complexes.

INTRODUCTION

Deciphering the behavior of histone tails within chromatin and its epigenetic modulation is essential to fully understand the detailed mechanisms that govern genome organization and influence gene expression regulation. In eukaryotic organisms, DNA and histone proteins self-assemble into nucleosomes that are connected by DNA linker segments and other architectural proteins including linker histones (LH).[1] The core histone proteins (H2A, H2B, H3, and H4) contain 10 positively charged protein regions, known as histone tails, that account for about a quarter of the histone core mass and extend from the nucleosome surface.[1a] It is believed that the histone tails affect chromatin compaction by mediating interactions with other proteins, nucleosomes, and linker DNAs.[2] Epigenetic changes, including methylation, ubiquitination, acetylation, and phos-

Received: April 20, 2015
Published: July 20, 2015

DOI: 10.1021/jacs.5b04086
J. Am. Chem. Soc. 2015, 137, 10205−10215

phorylation, exert their biological role by transforming chromatin structure, either directly[2c,d,3] or through the recruitment of other molecular species.[4]

The structure of the histone tails is only partially characterized crystallographycally.[5] Although this suggests a high degree of histone tail structural disorder, the extent of this disorder is unknown, and despite recent advances,[6] the detailed mechanisms of tail-induced chromatin compaction and epigenetic-driven changes remain obscure. Experiments assessing the structure of wild-type versus chemically modified histone tails within compact chromatin are challenging because of the highly crowded environment of chromatin and the difficulty of obtaining chromatin arrays with homogeneous histone tail compositions. Circular dichroism (CD) analyses have revealed that isolated H4 tail peptides display spectra characteristic of random coils,[7] that the total α-helical content of histone tails attached to their nucleosomes is approximately 17%, and that hyperacetylation of all core and tail histones increases the α-helical content by 64−100%.[7] A previous CD nucleosome study had reported a higher (30−35%) α-helical content in the tails of H3 and H4 and suggested that such folding is conditional upon DNA binding.[8] More recently, an amide hydrogen exchange and multidimensional NMR study of 12-unit compact oligonucleosomes suggested that the H3 tail is protected from solvent exchange.[6b] However, this study does not clarify whether the H3 tail has a defined secondary structure or whether it adopts a disordered but compact conformation; separately, it has been suggested that the histone tails in the highly condensed arrays could remain flexible yet simultaneously protected from solvent exchange on the relatively short exchange time scales investigated.[6a]

In contrast, a disordered histone tail behavior has been reported in a recent magic angle spinning (MAS) NMR spectroscopy study of condensed 177 base pairs (bp) 17-unit oligonucleosomes, which showed that residues 1−38 of H3 and at least 1−21 of H4 N-terminal tails are flexible and remain available for protein binding.[6a] Solution NMR measurements of the nucleosome with full histone tails demonstrated that all histone tail residues, except residues 16−22 of H4, have a disordered conformation in solution and that a mimic of K16 acetylation (K16Q mutation) disrupts the folded region of H4.[9] However, how well the K16Q mutation mimics K16Ac is controversial because, while the acetylated version opens chromatin, the mutation does not alter chromatin compaction.[2d,10] A combined CD and solution NMR study indicates that both isolated H4-tail peptides and hyperacetylated forms adopt extended and flexible structures.[11]

Computational studies of ever more complex biomolecules (e.g., ref 12) provide detailed views, as well as mechanistic and thermodynamic information, complementing experiments that might lack the spatial resolution to provide a molecular perspective of the problem. Hardware and software advances have allowed several all-atom simulations of isolated histone tails,[13] tails with DNA,[13a,14] and even nucleosomes[15] with explicit solvent and ions. All-atom molecular dynamics (MD) simulations in both implicit[16] and explicit solvent[13b] suggested that the histone tail peptides are not fully disordered. Indeed, a recent all-atom study has shown that H4K16Ac increases the histone tail/DNA binding affinity.[13a] Simulations of nucleosomes with tails have shown that truncation of the H3 or H2A tails alters the structure of the nucleosome core.[15b] Although insightful, the longest trajectories of nucleosomes with tails this far are about 100 ns,[15b] and those of isolated histone tails consist of replica exchange MD (REMD) studies with 60 ns of sampling per replica (or 3 μs of accumulated simulation time).[13b] Such level of sampling might not be sufficient to characterize histone tail structure and its role in internucleosome interactions (see Figure S1 showing lack of convergence at 150 ns). In fact, a multiscale approach is ideally needed to establish the conformational landscape of histone tails and relate it to changes in chromatin structure.[17]

Here we link the dynamics of wild-type histone tails and of lysine acetylated versions (a common epigenetic modification)[2c,18] to dinucleosome and oligonucleosome structure by an unparalleled multiscale approach[19] (see Figure 1 for an overview of our study and Tables S1 and S2 for the set of simulations performed). Our analyses indicate that while the wild-type tails are highly flexible and disordered, the dramatic increase of secondary-structure order by lysine acetylation unfolds chromatin by decreasing the tails' availability for crucial fiber-compacting internucleosome interactions. This molecular level description of the indirect structural effect of post-translational modifications of histones on chromatin organization explains the sequence sensitivity and underscores the delicate connection between local and global structural and functional effects. Our approach also opens new avenues for multiscale modeling of biomolecular complexes.

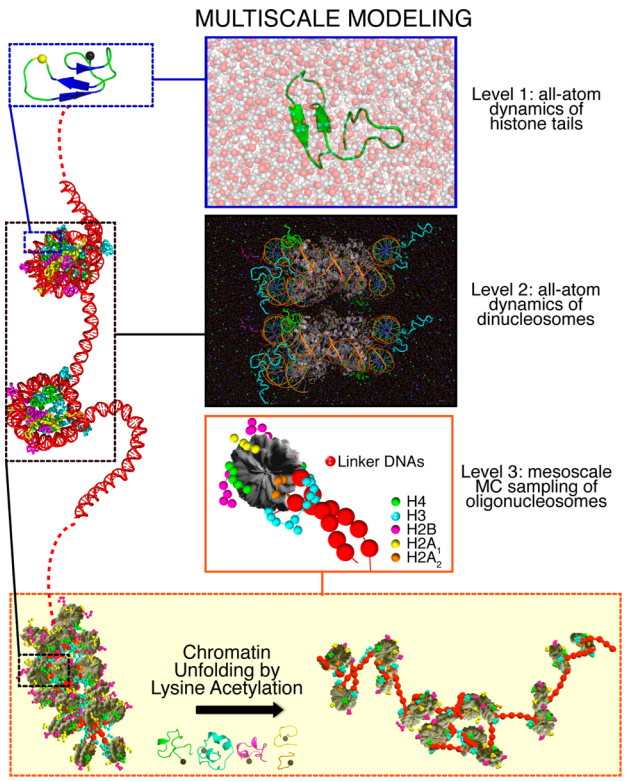

Figure 1. Overview of our multiscale computational study. We explore the behavior of histone tails, its epigenetic modulation, and its impact on chromatin compaction through a colossal multiscale study that combines multimicrosecond all-atom molecular dynamics simulations of dinucleosomes and histone tails with coarse-grained MC simulations of 24-nucleosome arrays. We describe a dramatic change in histone tail conformations due to lysine acetylation and reveal a tightly orchestrated physical mechanism by which such epigenetic modifications affect DNA accessibility.

DOI: 10.1021/jacs.5b04086
J. Am. Chem. Soc. 2015, 137, 10205−10215

METHODS

To examine the structure and behavior of histone tails and their effects on chromatin organization, we developed a multiscale computational protocol that combines all-atom MD simulations of dinucleosomes in explicit solvent (~800,000 atoms; 4 μs) and histone tails (aggregated time above 0.6 ms), with three state-of-the-art force fields and validated by experimental NMR data, with Monte Carlo (MC) coarse-grained modeling of chromatin fibers (24-nucleosomes). Our all-atom simulations comprise about 1 order of magnitude more sampling than previous studies, and our coarse-grained simulations study 80 different oligonucleosomes to extrapolate our all-atom findings into the nanoscale chromatin level. While the accuracy of atomistic models is needed for an adequate description of epigenetic marks, within chromatin their use is prohibitive due to the large number of degrees of freedom involved (e.g., a 50-nucleosome array without solvent contains more than 1 million atoms). Coarse-graining is one of the only alternatives to model chromatin because it can dramatically reduce the system dimensionality while maintaining essential physical and chemical information. Our multiscale approach exploits the advantages of both levels of modeling to perform a unique molecular-level analysis of the effects of lysine acetylation in chromatin structure.

All-Atom Studies. All our all-atom studies were performed in Gromacs 4.5[20] using explicit solvent and ions. Our simulations include 27 μs (accumulated sampling time per system) REMD simulations of the four N-terminal histone tails (H4, H3, H2B, and H2A), the C-terminal H2A tail (H2AC), five acetylated H4-tail states (H4K16Ac, H4K12Ac, H4K12,16Ac, H4K5,8,12Ac, and H4K5,8,12,16Ac), one acetylated H3-tail state (H3K14Ac), and two acetylated H2B-tail states (H2BK20Ac and H2B K5,12,15,20Ac). In addition, we performed 4 μs (accumulated sampling time) unrestrained simulations of dinucleosomes with wild-type tails and with H4K16Ac tails, and 1 μs unrestrained MD simulations of all wild-type histone tails. Periodic boundary conditions and the particle mesh Ewald method[21] for long-range electrostatics were used. We modeled the short-range repulsive and attractive dispersion interactions via a Lennard-Jones potential with a cutoff of 1.0 nm. We used the Settle algorithm[22] to constrain bond lengths and angles of water molecules and P-LINCS for all other bond lengths, with an integration time step of 2 fs. For the dinucleosome systems, we used virtual interaction sites[20,23] together with constraints between all bonded atoms to remove the hydrogen vibrations and allow a time step of 4 fs. The temperature was kept constant at 300 K by using the Bussi thermostat.[24] The pressure was kept constant and controlled by coupling the simulation box to a pressure bath of 1 atm.[25]

To select the most adequate force field for our study, we repeated our REMD simulations of the H4 and H4K16Ac tails with three different force fields, namely AMBER99SB*-ILDN,[26] AMBER99SB,[27] and CHARMM36,[28] and those of the other wild-type tails with two, AMBER99SB*-ILDN and AMBER99SB. In addition, we validated the H4 tail REMD ensemble against NMR chemical shifts (see below). We then selected the force field AMBER99SB*-ILDN to carry out the rest of the simulations. Force field parameters for acetylated lysines were taken from[29] for AMBER99SB*-ILDN and AMBER99SB (Papageorgiou's parameters) and from[30] for CHARMM36 (Dejaegere's parameters). To describe the nucleosomal DNA we used the AMBER99+parmBSC0[31] force field. We used the TIP3P model[32] to describe the water molecules. All simulations were done with 150 mM of sodium and chlorine ions, which were modeled using Dang's parameters.[33] Table S1 lists all MD simulations and force fields used in this work.

The initial structures for the wild-type histone tails and their acetylated versions were prepared using VMD[34] based on human sequences from the UniProt Consortium.[35] The lengths of the N-terminal tails H3, H4, H2B, and H2A were defined as the first 38, 26, 23, and 14 residues of each histone, respectively, as done previously.[13b] The C-terminal H2A tail was defined as the last 9 residues of the H2A histone. Isolated histone tails were not capped in the N- or C-terminus. The tails were placed in a simulation box large enough to host the proteins completely unfolded (distance to the wall was 1.2 nm) and immersed in water. The systems were energy minimized, then subject to 200 ps of restrained NVT simulation, and further equilibrated during 1 ns in the NPT ensemble. The systems were then simulated for 1 μs, starting with random velocities obtained from a Maxwell−Boltzmann distribution at 300 K. For the analysis of the simulations, we discarded the initial 100 ns as equilibration period. We used the program STRIDE[36] to determine the secondary structure adopted by the histone tails and measure the average time it takes for the different motifs to disappear. To define secondary structural elements, STRIDE uses empirically derived hydrogen-bond energies and compares $\varphi-\psi$ backbone torsion angles with the α-helix and β-sheet regions in a Ramachandran plot.[37] The parameters of STRIDE have been optimized based on visual assignments made by expert crystallographers of protein structures. α-Helices start when two consecutive amino acids have $i \rightarrow i + 4$ hydrogen bonds. The two edge residues are only labeled as belonging to the helix if they have adequate $\varphi-\psi$ angles, which implies that the minimum size of consecutive helical residues reported is three, not five. A similar definition is used for 3_{10}-helices but considering $i \rightarrow i + 3$ hydrogen bonds. β-sheets are assigned if at least two hydrogen bonds occur in the sheet with adequate $\varphi-\psi$ angles for the residues involved. From the output of STRIDE, we obtained the maps of folding propensity versus residue number by classifying the residues as being part of an (a) α motif if they belong to a group of three consecutive residues defined as either α- or 3_{10}-helix by STRIDE, or a (b) β motif if they belong to a group of two consecutive residues that are defined as an extended conformation by STRIDE.

The initial structures for our REMD simulations were taken from our unrestrained MD simulations described above. REMD simulations were performed using between 56 and 64 temperatures ranging from 300 to 450 K. The distribution of temperatures was chosen to guarantee an average exchange probability of 25%, with the aid of the temperature predictor of Patriksson and van der Spoel.[38] The exchanges between neighboring replicas were attempted every 50 ps. Each system was simulated for 500 ns. The initial 100 ns were discarded in the subsequent analysis. We then analyzed the lowest temperature replica data with the program STRIDE[36] to determine if the histone tails adopt α or β structure, as define above. Following this, we reshuffled the data and divided it in 40 ns subensembles to compute the average and the standard deviation of the propensity of each residue to form either α or β motifs among the subensembles. In addition, for each histone tail we performed RMSD clustering as implemented in the program g_cluster in Gromacs 4.5[20] using a total of 25,000 structures collected at 20 ps intervals from the lowest temperature replica and a cutoff of 0.2 nm. For this, external translational and rotational motions were removed by minimizing the RMSD distance of the C_α atoms with respect to those of the first frame.

To probe the conformational dynamics of wild-type and acetylated (H4K16Ac) histone tails in a nucleosomal environment, we performed two sets of dinucleosome simulations each with a different starting H4/H4 K16Ac setup. For the two sets, we stacked two nucleosome particles (X-ray structure with PDB code 1KX5)[39] on top of each other following the positions and orientations of stacked nucleosomes in the tetranucleosome crystal (X-ray structure with PDB code 1ZBB).[40] For consistency with our REMD studies, the H4/H4 K16Ac tail sequences were replaced with the human ones. In the first setup, we attached an extended H4 structure from our REMD ensembles to each nucleosome and oriented it to ensure that its N-terminal region was placed near the acidic patch of its neighboring nucleosome (Figure 4a). In the second setup, the H4 tails were oriented toward the nucleosomal DNA (Figure 4b). The dinucleosome systems were embedded in a truncated octahedron box containing 203,778 water molecules, leaving 2 nm between the nucleosome atoms and the edges of the box. This separation is large enough to accommodate a fully extended H3 tail, which is the longest one. We added 895 sodium ions and 601 chlorine ions to balance the nucleosome charge and give an ionic concentration of 150 mM NaCl. Each dinucleosome system was energy minimized and simulated twice (two different random seeds) for 500 ns. The first 100 ns of each trajectory were discarded.

DOI: 10.1021/jacs.5b04086
J. Am. Chem. Soc. 2015, 137, 10205−10215

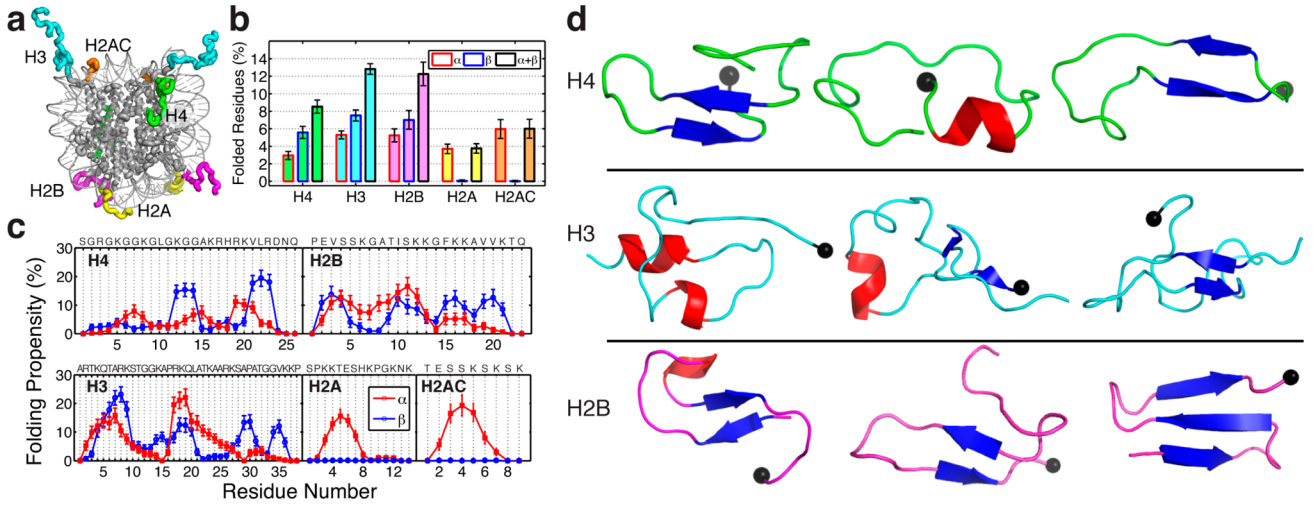

Figure 2. Transient secondary structure populations in the wild-type histone tails. (a) Illustration of histone tails (H4 in green, H3 in blue, H2B in magenta, H2A in yellow, and H2AC in orange) extending out of the nucleosome surface (PDB 1KX5). (b) Ensemble average and standard deviation (SD) of the percentage of residues in each of the different histone tails calculated from the last 400 ns of the 300 K REMD trajectory (SD computed by block average using 40 ns windows). The percentages of residues forming α-helices (red exterior line), β-strands (blue exterior line), and their sum (black exterior line) are shown separately. (c) Folding propensity, i.e., fraction of configurations that each residue adopts α-helical (red) or β-strand (blue) structural motifs. The sequence for each tail is shown. (d) Illustration of cluster with the highest population with folded residues for H4 (first cluster with 12.54% population, ninth with 2.49%, and 11th with 2.00%), H3 (first with 4.15%, third with 3.77%, and fourth with 3.75%), and H2B (second with 9.08%, fifth with 3.08%, and %, and sixth with 2.00%). The α-helical motifs are colored in red, while β conformations are in blue. The black sphere indicates the last residue of the N-tail (point of attachment to the nucleosome).

Validation of All-Atom Studies Using NMR Chemical Shifts. We performed two-types of validations of our simulation ensembles using experimental NMR chemical shifts of the histone tail H4 (residues 1 to 15) and the H4K16Q mutation (residues 1 to 17) attached to their nucleosomes.[9] The chemical shifts are available for all the C_α, and amide N and H backbone atoms, and the C_β atoms. First, we used the experimental data to perform replica-averaged chemical shift restrained MD simulations and generate an ensemble of structures to compare against our REMD results.[41] Second, we used the predictor delta2D (δ2D)[42] to calculate the propensity of the H4 tail to form α or β secondary structures based on the experimental chemical shifts and compare against the folding propensities resulting from our REMD ensembles.

In the replica averaging procedure, a set of chemical shifts were computed with the Camshift[43] method using the coordinates of the atoms for which chemical shifts are available and averaging over 8 replicas. The chemical shift restraints are implemented in the Gromacs engine via the Plumed[44] package and the Camshift algorithm. A quadratic potential based on the differences between the reference and the computed average chemical shift is added as external penalty. The strength of the interaction was adjusted to the highest possible value that did not affect the stability of the trajectories.[41] Two replicas were biased using the metadynamics scheme,[41,45] employing a time-dependent energy deposition that helps overcome conformational barriers. In one replica, we deposited Gaussian-shaped potential energies every 500 MD steps (1 ps) on the underlying force-field energy landscape based on the end-to-end distance of the H4 chain using a Gaussian width of 0.1 nm and height of 0.1 kJ/mol. In another independent replica we deposited energy with the same frequency on the collective coordinate calculated as the number of hydrogen bonds between all donors and acceptors. In this case, the height of the Gaussian was also 0.1 kJ/mol, and the width was 0.5 hydrogen bonds. We used a continuous expression for the number of hydrogen bonds that involves counting the resulting product of two functions that quickly drops from 1 to 0 at a cutoff value A_0 for each possible hydrogen bond. Each individual function is evaluated as $(1 - (A/A_0)^6/(1 - (A/A_0)^{12}$. For each hydrogen bond, the distance between the hydrogen and the acceptor ($A = d$) has a cutoff at $A_0 = d_0 = 0.3$ nm, and the angle between the hydrogen-donor and hydrogen-acceptor vectors ($A = \alpha$) has a cutoff at $A_0 = \alpha_0 = 0.66\pi$. Finally, we estimated the secondary structure content in these restrained simulations and compared against our REMD results.

Histone Tail Flexibility. To compare the relative flexibilities between wild-type histone tails and their acetylated version, we computed the tails' persistence lengths L_p. The persistence length is a common measure of protein flexibility: the lower the persistence length, the higher the flexibility. While, in statistical terms, systems with contour lengths, L, that satisfy $L \ll L_p$ are rigid and maintain an average straight conformation with a preferred tangent direction, systems with $L \gg L_p$ are flexible and bend spontaneously. Systems in which L is comparable with L_p are considered semiflexible, and their structural rearrangements are determined by the competition of the thermal energy and the bending rigidity. For each tail, we computed the persistence length from the lowest temperature replica based on the projection of the end-to-end vector ($\mathbf{R}$) with respect to its initial direction (r_1),[46] as follows

$$L_p = \left\langle \frac{r_1}{l}\cdot\mathbf{R} \right\rangle = \frac{1}{l}\sum_{i=1}^{N-1}\langle r_1\cdot r_i\rangle = \sum_{i=1}^{N-1}\langle |r_i|\cos\theta_{1i}\rangle \quad (1)$$

Here r_i is the vector joining the i^{th} and $(i + 1)^{th}$ C_α atom, l is the distance between C_α atoms ($l = 0.38$ nm), and N is the total number of residues in the histone tail. To compute θ_{1i}, the angle between vectors r_1 and r_i, we used the program g_sgangle in Gromacs 4.5.[20] We define the contour length of the tails as the number of amino acids in each tail multiplied by l. An illustration of the definition of the persistence length is given in Figure S2.

Chromatin Coarse-Grained Simulations with Flexible and Folded Tails. To link our all-atom findings to the level of nanoscale chromatin, we carried out oligonucleosome coarse-grained simulations that explore the effects of histone tail folding. These coarse-grained studies compare the behavior of 24-nucleosome systems without LH and two different DNA linker lengths (35 and 62 bp) with eight different concentrations (0, 5, 10, 25, 50, 75, 90, and 100%) of folded histone tails. In addition, we also include simulations in which we have reduced the charge of the H4 and H3 tails by 1e due to monoacetylation but kept the flexibility unaltered. Our coarse-grained model[17a−c,e,47] captures several key features of chromatin fibers, including electrostatics, DNA and nucleosome mechanics, structural irregularity, and histone tail flexibility, and averages out other effects

DOI: 10.1021/jacs.5b04086
J. Am. Chem. Soc. 2015, 137, 10205−10215

like protein/DNA sequence effects, hydrogen bonding, atomistic fluctuations, and solvation. In essence, our model represents the nucleosome with wrapped DNA but without histone tails as an electrostatic object with Debye−Hückel charges;[47a,c] DNA linkers are described as chains of charged beads by a combined worm-like-chain model;[48] histone tails are treated as chains of charged beads with parameters that mimic their atomistic behavior;[17b] and sampling of phase space is achieved through a MC algorithm. Unfolded histone tails are described as flexible worm-like chains using our original model.[17a] In addition, transient populations of folded tails are incorporated as almost rigid entities with equilibrium configurations taken from the highest populated folded structure obtained for each tail in the lowest temperature replica of our REMD simulations. Specifically, to model folded tails, as done in our original model, we assign one bead per each five amino acids, center the bead at the C_β atom of the middle amino acid, and assign to each bead the total charge of the five amino acids it represents. An image showing the histone tail beads overlaid on top of all-atom histone tails (extended and folded) and giving the sequence of amino acids grouped in each bead and the bead charge is presented in the Figure S3. To limit tail flexibility, we increase the stretching, bending, and torsional intertail-bead force constants by a factor of 100. Despite being almost rigid, the tails can spontaneously fold/unfold through a tailored MC move (see Supporting Information) that attempts transitions between folded and flexible tails. This allows us to explore the whole conformational ensemble of oligonucleosomes with a given percentage of folded tails. For our additional simulations exploring the effects of charge reduction due to acetylation, we have decreased by 1e the charges of the tail beads that contain residues H4K16 and H3K14 but have kept the flexibilities of the tail unaltered. The simulations were performed at physiological conditions; this is, a temperature of 298 K and a high monovalent salt concentration of 150 mM NaCl. Every simulation set includes 12 trajectories that cover the mean DNA twist angle and twist deviations of +12 and −12° about the mean twist to mimic natural variations, as done previously.[17c] Each simulation trajectory was run for up to 50 million MC steps. The last 5 million steps were used for statistical analysis. Convergence of these simulations is reached well before 45 million MC steps as shown elsewhere.[17c] For our initial configurations, we use representative zigzag equilibrium conformations for oligonucleosomes with flexible tails obtained previously.[17c] For more details on our coarse-grained model see refs 17b, c, and 47e and the Supporting Information.

RESULTS

Histone Tails Are Structurally Highly Heterogeneous. Our massive REMD simulations of the five different isolated histone tails in explicit solvent (Table S1) confirm that histone tails are mostly unstructured and exhibit only transient secondary structural elements.[6a,9,13b,16b] The conformational ensembles obtained at physiological conditions (150 mM monovalent salt and room temperature) contain only a small (<15%) fraction of residues with α-helical or β-strand conformations (Figure 2a). For the H4 tail, the most abundant structure is an antiparallel β-hairpin (KGG 12−14 and VLR 21−23) connected by a six-residue loop with four positively charged residues (15−20 AKRHRK). The H4-tail transient α-helical motifs and the α-helical/β- motifs for the rest of the tails are short (i.e., formed by only 3−6 residues per tail) and highly diverse (i.e., many different motifs are formed by combinations involving most residues), which illustrate the overall structural disorder of histone tail conformations. Figure S4 provides examples of the most populated folded structures with higher atomic detail. These motifs are compact and able to fit within a compact dinucleosome structure (see Figure S5), short-lived (i.e., ∼48 and 88 ps for α-helical and β- strand H4 structures, respectively), and highly heterogeneous (Figure 2b,c). Estimated persistence-to-contour-length ratios from the MD ensembles (see Table S3) measure the length scale over which histone tails remain relatively straight. Even though the tails adopt transient secondary structural elements, their persistence-to-contour-length ratios are smaller than one. Thus, histone tails are flexible and display a high degree of histone tail bending from thermal fluctuations (Table S3). The persistence lengths we obtain for the five histone tails are consistent with experimental values of flexible random coiled proteins of similar sizes (0.48—0.63 nm) and 1 order of magnitude smaller than that of polyproline (4.4 nm) which is considered the stiffest homo-oligopeptide[49] (Table S3). The histone tail values are also much smaller than the measured persistence lengths of DNA (50 nm)[50] and chromatin fibers (diverging between 30 and 200 nm[51]), highlighting their high flexibility within the chromatin context.

To control for the effects of the specific force fields used in the simulations, we repeated the simulations for the H4 tail with three different state-of-the-art force fields (see Tables S1 and S2) and validated the resulting ensembles using chemical shifts of histone tails measured for reconstituted nucleosomes.[6b] Calculations with the different force fields reveal nearly identical results (Figure S6). Our simulations agree well with the experimental data that shows that folding of H4 deviates from a fully random coil behavior (Figure S6). For further control, the atom-type-averaged chemical shifts calculated from our H4 tail ensembles also deviate from a complete random coil sequence-based prediction.[52] Furthermore, the folding propensities obtained with our additional restrained simulations that satisfy the experimental chemical shifts and those from our REMD simulations with the AMBER99SB*-ILDN[26] force field deviate from the folding propensities calculated using experimental chemical shifts almost identically.

Epigenetic Modifications Can Change Histone-Tail Flexibility. REMD simulations of acetylated H4, H3, and H2B tails examine how the tails' structure and behavior is altered by lysine acetylation. We focus on these three tails because they have been reported to be most influential in chromatin architecture regulation[53] and on lysine acetylation because this important modification for gene regulation is commonly present in transcriptionally active chromatin and is thought to directly affect chromatin structure.[18] For instance, hyperacetylation of histones is present in open sea urchin chromatin (with linker DNAs of 61 bp)[54] and correlates with decondensed yeast chromatin (∼18 bp linker DNAs[55]).[56] In addition, monoacetylation is associated with both open chromatin (H4K16Ac),[2c,d] and with silent and compact chromatin (H4K12Ac).[57]

Lysines are present in four H4-tail residues (5, 8, 12, and 16), seven H3-tail residues (4, 9, 14, 18, 23, 27, and 36), and six H2B-tail residues (5, 11, 12, 15, 16, and 20). Among all the possible mono and polyacetylated states, we study two monoacetylated (K12Ac and K16Ac) and three polyacetylated states (i.e., K12 and 16Ac, K5, 8, and 12Ac, and K5, 8, 12, and 16Ac) for H4; for H3, we study one monoacetylation (K14Ac); and for H2B one monoacetylation (H20Ac) and one polyacetylation (K5,12,15,20Ac) (see Table S1 for a list of all cases analyzed). Comparing H4K16Ac versus H4K12Ac allows us to determine whether lysine acetylation has a sequence specific effect. We analyze H3K14Ac and H2BK20Ac because their presence is correlated to transcription activation.[58] Finally, we study the polyacetylated states to analyze the additivity or cooperativity properties of lysine acetylation.

DOI: 10.1021/jacs.5b04086
J. Am. Chem. Soc. 2015, 137, 10205−10215

We find that K16Ac increases the overall propensity of H4 residues to adopt both α-helical and β-strand conformations by about 50% (Figure 3a) and increases the persistence length by

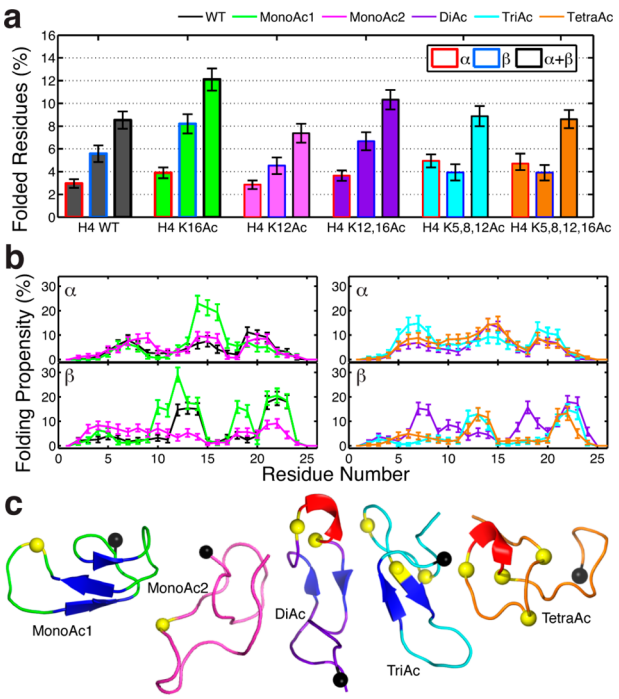

Figure 3. Effect of the acetylation of different lysine residues in the H4 tail. (a) Percentage of residues in various lysine-acetylated tails with secondary structure motifs. (b) Effect of acetylation in the folding propensity for each residue separated by α-helical and β strand structural motifs. (c) Illustration of highest populated clusters with folded resides. α-Helical motifs are colored in red, while β conformations in blue. The black sphere indicates the last residue of the N-tail (point of attachment to the nucleosome), while the yellow sphere denotes the acetylated lysine.

41%, thereby decreasing the flexibility of the tail (Table S4), consistent with previous theoretical suggestions[13a] and with CD data showing that lysine acetylation of all core and tail histones increases the α-helical content of the nucleosome by 64–100%.[7] An illustration of the larger space covered by H4 versus H4K16Ac during a 1 μs-long MD simulation is shown in Figure S7.

The greater effect of H4K16Ac over H4K12Ac as well as the polyacetylated states (Figure 3a,b) suggests that acetylation effects are sequence dependent, nonadditive, and not explained by histone charge reduction alone. Namely, acetylation dramatically increases not only the α-helical propensity of K16 but also of the two residues preceding it (14–15), from around 7% to 21%. The stabilization of this three-residue α-helix brings residues 10–12 and 18–19 closer together, favoring a β-hairpin conformation not observed in the wild-type H4 (Figure 3c). We also observe that acetylation increases slightly the β-strand propensity of residues 12–14 and 21–23, due to the stabilization of both the β-hairpin loop (mainly formed by positively charged residues) and the N-termini-to-C-termini partially negative-to-partially positive dipole in residues 12–16 (KGGAKAc). Thus, removal of the positive charge upon acetylation turns K16 into a more efficient C-terminal cap for the β-hairpin that H4 transiently samples and allows stronger dipolar interactions among the two β strands.[59] By contrast, K12Ac decreases formation of β-hairpins, possibly due to the destabilization of the overall β-strand dipole. Consistently, the K12,16 diacetylation increases the propensity for folding compared to the wild-type tail, but decreases it compared to K16Ac alone. The tri- and tetraacetylated cases show similar structural patterns with a preference toward α-helix formation and a similar total folding compared to the wild-type tail. For H3 and H2B, the monoacetylations analyzed do not change tail behavior significantly, but the H2B tetraacetylation increases notably helicity and stiffness of H2B (see Supporting Information and Figure S8); these observations further support the sequence-dependent role of lysine acetylation.

A Decrease of Histone Tail Disorder Limits Internucleosome Interactions in Dinucleosomes. Our 1 μs explicit-solvent all-atom dinucleosome simulations (Figure 4) investigated the role of histone tails in dinucleosome interactions by comparing the number of histone tail-mediated nucleosome–nucleosome contacts between two stacked nucleosomes with wild-type versus H4K16Ac tails. Our dinucleosome models were built using the positions and orientations of two stacked nucleosomes in the tetranucleosome crystal. As observed in Figure 4, the two nucleosomes are laterally displaced with respect to each other, mimicking the disposition of nucleosomes in experimentally based chromatin models.[40,60] We have explored two simulation setups, each with a different starting configuration of the H4 tails. In the first setup (setup a; Figure 4a), the H4 tails extend from their point of attachment on their parent nucleosome to the acidic patch of their neighboring nucleosome; this setup is expected to occur within compact chromatin. In the second setup (setup b; Figure 4b), the H4 tails extend from their point of attachment on their parent nucleosome toward the nucleosomal DNA. Our simulations reveal that the dinucleosome with wild-type tails in setup a, in which the H4 tails can interact with their neighboring acidic patch within the time scale of our simulations, are stabilized by 40% more internucleosome interactions than that in setup b.

For both setups, the average number of H4-mediated internucleosome contacts—the sum of tail contacts with the neighboring DNA and with the neighboring proteins—decreases significantly in the presence of H4K16Ac (by 119 contacts in setup a, and by 77 contacts in setup b; Figure 4c). The total number of DNA/H4 tail contacts is not notably altered upon acetylation (Figure 4c), suggesting that acetylation decreases the ability of the H4 to extend and reach the neighboring nucleosome but not the binding affinity of the H4 tail with the DNA. An all-atom umbrella sampling study of H4 with DNA had showed that the free energy stabilizing the DNA/H4 bound states increases upon K16 acetylation.[13a]

Histone Tail Folding Triggers Chromatin Fiber Opening. Changes in the structure of histone tails can dramatically impact chromatin organization since the tails provide crucial bridging interactions with the charged surfaces of neighboring nucleosomes (nonparental nucleosome) and the linker DNAs joined to other cores (nonparental linker DNA). Clearly, many factors affect chromatin structure in a cooperative way. Indeed, different internal and external factors favor different fiber organizations,[61] and a fluid polymorphic structure, including irregularly folded 10 nm fibers, is more consistent with the heterogeneous conditions of in vivo chromatin.[17e,62] The length of the DNA linking consecutive nucleosomes is an important factor affecting chromatin organization, and its effects are

DOI: 10.1021/jacs.5b04086
J. Am. Chem. Soc. 2015, 137, 10205–10215

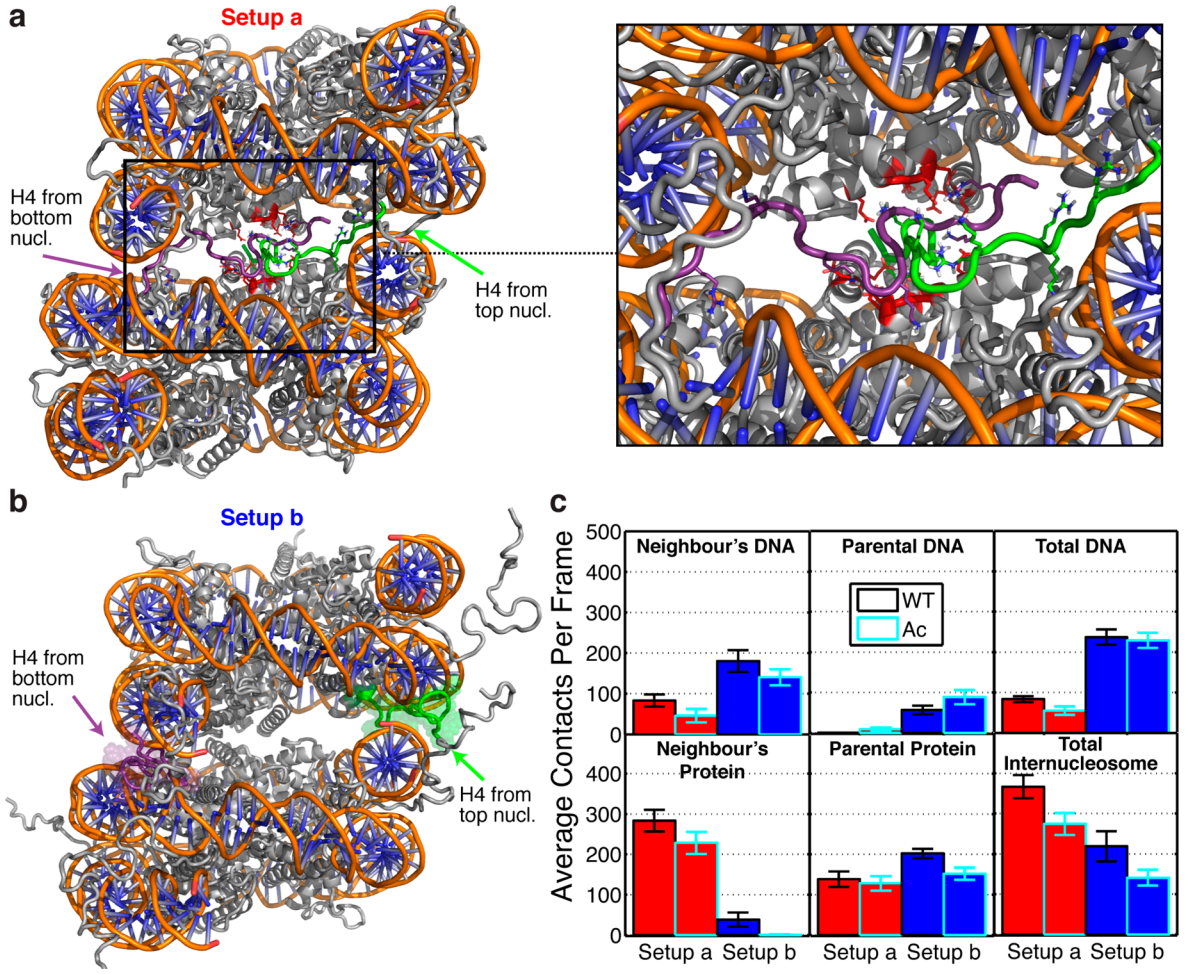

Figure 4. Internucleosome interactions within dinucleosomes mediated by the H4 tail and its monoacetylated H4K16Ac version. (a) Illustration of the first simulation setup (setup a). The H4 tails extend from their point of attachment in their parent nucleosome toward the acidic patch of their neighboring nucleosome. The H4 tail of the top and bottom nucleosomes are highlighted in green and purple, respectively. At the right, we zoom in into the acidic patch region highlighting the acidic patch residues in red (H2A: E56, E61, E64, D90, E91, E92 and H2B: E102, E110) and showing the positive H4-tail residues with sticks but omitting nonpolar hydrogens for clarity. (b) Illustration of the second simulation setup (setup b). The H4 tails extend from their point of attachment in their parent nucleosome toward the nucleosomal DNA. (c) For both setups, total number of histone tail-DNA/protein contacts (tail and DNA atoms closer than 0.3 nm) mediated by the wild-type H4 tail (WT) versus the acetylated version (Ac) separated as tail/DNA of neighboring nucleosome (Neighbor's DNA), tail/DNA of parent nucleosome (Parental DNA), total neighboring + parent tail/DNA (Total DNA), tail/protein of neighboring nucleosome (Neighbor's Protein), tail/protein of parent nucleosome (Parental Protein), tail/total (neighboring DNA + neighboring protein; Total Internucleosome). The red bars show the results for setup a and the blue bars the results for setup b. The bars corresponding to dinucleosomes containing wild-type or acetylated H4 versions have black and cyan borders, respectively.

intertwined with LH presence, ionic conditions, and others.[17c,e,47e,63] The linker DNA length varies within and across species, tissues, cell-cycle states, and even within single chromatin arrays. While transcriptionally active cells are characterized by short-to-medium linker DNA lengths of ∼7−42 bp, mature inactive cells have medium-to-long values of ∼43−93 bp.[63b] Linker DNA variations also change the way in which histone tails interact with other chromatin components and thus affect chromatin structure overall.[17c,e,63a]

Our oligonucleosome coarse-grained model[17a−c,e] (see Methods section, Figure 5a, and Supporting Information), which has been developed and validated over the past 10 years,[17a−c,e,47] has a DNA−DNA interbead separation of ∼9 bp and can thus treat chromatin with linker DNA lengths of 26, 35, 44, 53, 62 bp, etc. Using this model we compare the degree of compaction of 24-nucleosome arrays without LH (more relevant to acetylation)[2d] under physiological conditions of monovalent salt and two different linker DNA lengths (35 and 62 bp, corresponding to nucleosome repeat lengths of 182 and 209 bp, respectively). We analyze 80 different fibers with different distributions of folded-and-semirigid/unfolded-and-flexible tails mimicking our all-atom findings to help characterize how transient secondary structural elements in the different histone tails impact chromatin compaction.

We find that the H3 and H4 wild-type histone tails have dominant roles in mediating internucleosome interactions (Figure S9). Figure 5b reveals that for the two different types of chromatin arrays analyzed (linker DNAs lengths of 35 bp and 62 bp), even a small presence of folded histone tails (>5%) induces chromatin fiber unfolding. Thus, structure-rich collapsed histone tails, for example by H4K16Ac, are consistent with weaker internucleosome contacts and accordingly poorer chromatin compaction.

We also see that chromatin decondensation due to histone tail folding is linker-DNA length dependent. For 62-bp DNA linkers, histone tail folding has an additive effect on chromatin

DOI: 10.1021/jacs.5b04086
J. Am. Chem. Soc. 2015, 137, 10205−10215

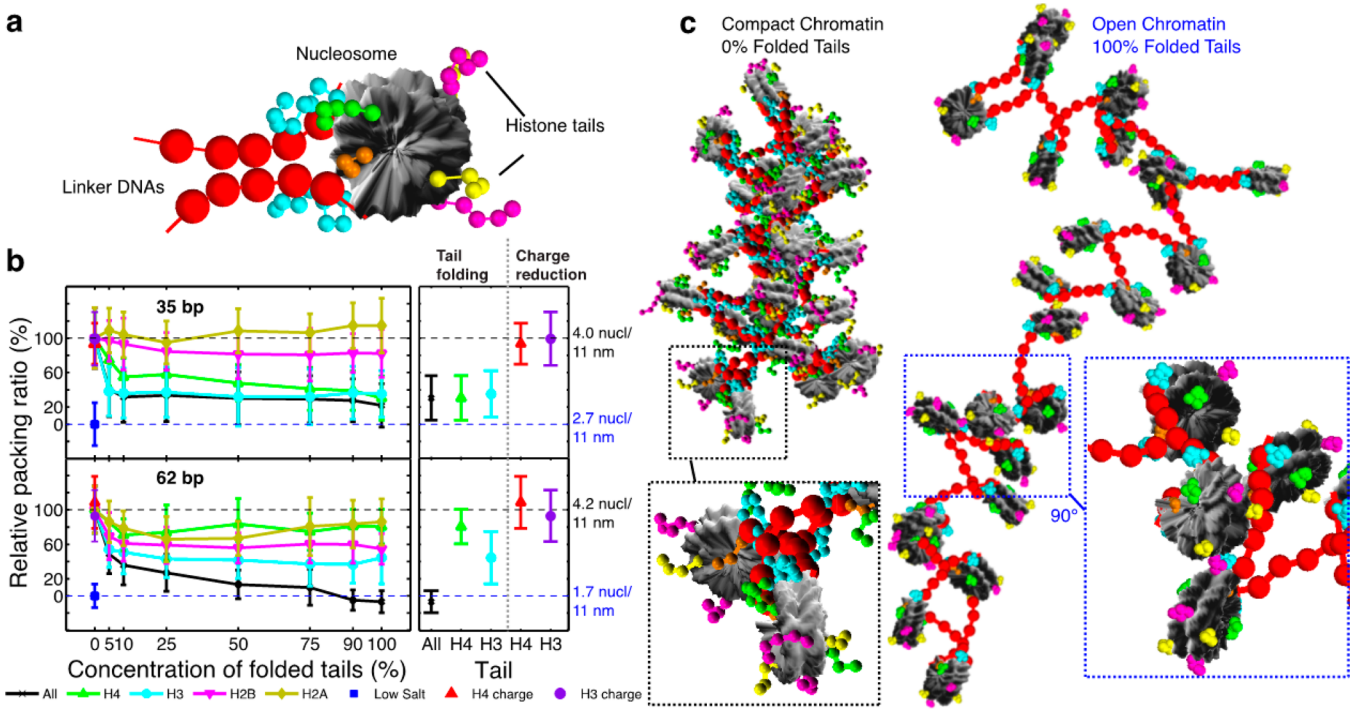

Figure 5. Analysis of the effects of the folding of the histone tails on the compaction of chromatin fibers. (a) Illustration of the coarse-grained model; nucleosome-charged surfaces are shown in gray, linker DNA beads in red, and histone tail beads in green (H4), cyan (H3), magenta (H2B), yellow (H2A), and orange (H2A C-tail). (b) Effects of histone tail folding concentration on the compaction of chromatin measured through packing ratios of 24-nucleosome system with two different linker-DNA lengths (35 and 62 bp). The left section of the graph describes how the relative packing ratio (see Supporting Information) decreases as the concentration of the folded tails increases. The relative packing ratios varies between 0% for a fully unfolded fiber at low salt concentrations (10 mM NaCl) and 100% for a compact conformation at physiological salt (150 mM NaCl) and no folded tails (0% folded tails). The right section of the graph compares the effects of having 100% folded tails (black: all tails, green: H4 tail, or cyan: H3 tail) or reducing the charge by 1e to mimic the effect of acetylation but keeping the tails fully flexible. (c) Simulation snapshots for the 62-bp linker-DNA system with fully folded and flexible tails.

decondensation; fiber opening requires the simultaneous folding of various types of histone tails, with H3- followed by H2B-tail folding being the most influential. When >50% of all histone tails are folded, the opening effect is similar to immersing the fibers in a low salt environment (Figure 5c). Indeed, these fibers with fully folded histone tails show no salt-dependent compaction. Although the structure of 35-bp linker-DNA chromatin is more resistant overall to histone tail folding, due to higher mechanical constraints imposed by the shorter linker DNAs, folding of either H4 or H3 tails can decrease the compaction to near low-salt values. A 30% presence of H4 K16Ac has been shown to be sufficient to almost fully decompact chromatin without LH[2d] and a 55-bp linker-DNA.

For both linker DNAs, we verified that the crucial reduction of internucleosomal contacts we observe is not to charge reduction per se by repeating calculations for wild-type histone tails conformations, where the bead charges corresponding to H4K16Ac or H3K14Ac were reduced by 1 e to mimic charge neutralization due to lysine monoacetylation. Charge reduction did not change the computed packing ratios (Figure 5c), suggesting that epigenetic marks, such as lysine acetylation, do not induce fiber decompaction through charge neutralization per se, but through a cooperative multiscale mechanism involving the dramatic reduction of crucial stabilization of internucleosome interactions due to unavailability of flexible histone tails for potential contacts. Thus, we expect that other factors that enhance tail order and limit their availability, like protein binding, will have similar effects.

DISCUSSION

Using a tailored multiscale modeling approach, we show that wild-type histone tails are highly flexible and mostly disordered protein regions and that these characteristics of histone tails facilitate contacts with nonparent nucleosomes because unstructured tails have larger interaction surface areas, and thus more potential binding opportunities. In addition, despite being mostly unstructured, wild-type histone tails adopt a wide range of different transient and short secondary structural motifs that might facilitate binding to various molecules (e.g., histones, DNA, and chromatin remodellers) through a conformational selection mechanism. Thus, histone tail disorder and flexibility are crucial regulators of chromatin structure, not only by affecting internal interactions but also recruitment of other molecules. Another important aspect of histone tail flexibility and disorder is to ensure that a larger fraction of the tail residues are exposed to the solvent, where they are more readily available to epigenetic-modifying enzymes.

Our studies also reveal that lysine acetylation decreases the tail's flexibility and increases their secondary structure folding propensity in a sequence-dependent manner. Indeed, although charge reduction by polyacetylation is greater, H4 polyacetylation of lysines 5, 8, 12, and 16 has a negligible effect in the characteristics of the tails, when compared to single K16 acetylation. Our dinucleosome simulations combined with our coarse-grained modeling further reveal that the structuring effect of lysine acetylation limits the ability of the tails to

DOI: 10.1021/jacs.5b04086
J. Am. Chem. Soc. 2015, 137, 10205−10215

extend, reach nucleosome neighbors, and establish a range of crucial protein−protein and protein−DNA chromatin-compacting internucleosome interactions. This compromise leads to chromatin fiber opening.

Our results agree with a study that combines short (60 ns per replica) REMD of H4 and H4K16Ac tails in explicit solvent with umbrella sampling simulations of DNA/tail systems and demonstrates that such modification decreases the tail disorder and increases the tail/DNA bind affinity.[13a] The study further hypothesizes that K16Ac might induce chromatin decompaction through increase of the tail/parental DNA interactions and the sequestration of the H4 tail into its own nucleosome. Our dinucleosome simulations reveal that H4K16Ac limits the interactions of the tail with both the neighboring protein and DNA, and our coarse-grained simulations demonstrate that enhanced rigidity of the histone tails decreases the compaction of the chromatin fiber dramatically.

In addition, we find that the effect of acetylation in tuning fiber compaction is linker-DNA dependent. Our coarse-grained model suggests that H4 modifications that reduce the tail's flexibility have a stronger effect in chromatin with shorter linker DNAs (<62 bp) without LHs, while modifications of H3 tails will affect longer linker DNA arrays more strongly. This can be explained by the position and length of these histone tails. The H4 tail is more important for short linker DNAs because of its optimal position on the nucleosome surface, while the much longer H3 tail can reach its nonparental DNA and nucleosome neighbors more easily when they are further away in longer NRL fibers. This is consistent with experiments showing that H4K16Ac is present in decondensed yeast chromatin (linker DNA ∼18 bp[55]),[56] where 80% of H4K16 residues are acetylated,[56] and in active male-X *Droshopila* chromosomes (linker DNA ∼43 bp[64]),[65] while H4K12Ac is preferentially found in compact yeast chromatin.[57] Furthermore, within the H4 tail, residues 14 to 24 of H4 are essential for the condensation of 30-bp linker-DNA chromatin arrays.[66] H4K16Ac also opens chromatin fibers in 20-bp linker DNA 12-unit reconstituted arrays[2c] and in 55-bp linker DNA 60-unit arrays in the absence of LHs.[2d]

CONCLUSION

Our multiscale study sheds light into the structure and dynamics of the histone tails and identifies a mechanism by which epigenetic modifications can modulate the degree of compaction of chromatin and the corresponding accessibility of the DNA. Our results suggest that the disordered nature of wild-type histone tails controls chromatin compaction and promotes the recycling of the same histones to recruit a range of different molecular partners. Structural disorder and flexibility thus allows histone tails to perform two crucial functions: (a) contact neighboring nucleosomes and linker DNAs to directly promote chromatin compaction, and (b) interact with nonhistone proteins for indirect chromatin structure regulation.

That the flexibility of histone tails, which favors internucleosome interactions, can be decreased by lysine acetylation to induce different levels of global chromatin decondensation underscores that this increased structural order of the tails upon acetylation is not merely a charge reduction phenomenon, but a subtle sequence-specific effect. Thus, the decrease of internucleosome interactions through acetylation is due to the inability of the structured histone tails to extend and reach their neighboring nucleosomes, rather than reduced binding with DNA.[67] Furthermore, we propose that the effects of acetylation on chromatin compaction are linker DNA-length dependent, with H4 modifications being most important for short-to-medium linker DNAs (<62 bp), and H3 modifications being most important for medium-to-long linker DNAs (>62 bp).

Taken together, our multiscale computational results reveal a molecular mechanism by which an epigenetic modification of the histone tails controls chromatin structure. This key role of histone tail flexibility on chromatin compaction might also help explain how molecules that remodel chromatin by binding to the tails might act to modify gene expression. These results provide a compelling illustration of the manner by which subtle modifications of the molecular structure of histone tails can profoundly impact chromatin structure and in turn gene expression. Our work also opens new avenues for multiscale computations of complex biological systems.

ASSOCIATED CONTENT

Supporting Information

Descriptions of our coarse-grained model, MC simulation approach, calculation of chromatin packing ratios and tail-mediated internucleosome interaction frequencies. It also contains four tables and eight figures. The Supporting Information is available free of charge on the ACS Publications website at DOI: 10.1021/jacs.5b04086.

AUTHOR INFORMATION

Corresponding Authors

*modesto.orozco@irbbarcelona.org
*schlick@nyu.edu

Author Contributions

#These authors contributed equally.

Notes

The authors declare no competing financial interest.

ACKNOWLEDGMENTS

We thank the Bai group for sharing with us their NMR chemical shifts, and Dr. Annick Dejaegere for sending us CHARMM parameters for lysine acetylated residues. Computing support from the Barcelona Supercomputing Centre MareNostrum Supercomputer and from New York University High Performance Computing Union Square cluster is acknowledged. We are grateful with David Vicente, Head of User Support at the Barcelona Supercomputing Center, for his extensive help with MareNostrum. This work was supported by the European Union Seventh Framework Programme (FP7/2007−2013) [275096 to R.C.-G. and M.O.]; the European Union's Horizon 2020 research and innovation programme under a Marie Sklodowska-Curie grant [654812 to G.P. and M.V.]; Sara Borrell Fellowships [to G.P. and M.O.]; the Spanish MINECO [BIO2012−32868 to M.O.]; the Spanish National Institute of Bioinformatics (INB) [to M.O.]; the European Research Council (ERC) [Advanced Investigator Grant to M.O.]; the National Science Foundation [MCB0316771 to T. S.]; the National Institutes of Health [R01 GM55164 to T. S.]; Philip Morris USA [to T. S.]; and Philip Morris International [to T.S.]. M.O. is an ICREA-Academia fellow.

DOI: 10.1021/jacs.5b04086
J. Am. Chem. Soc. 2015, 137, 10205−10215

REFERENCES

(1) (a) Luger, K.; Mader, A. W.; Richmond, R. K.; Sargent, D. F.; Richmond, T. J. *Nature* **1997**, *389* (6648), 251−260. (b) Richmond, T. J.; Davey, C. A. *Nature* **2003**, *423* (6936), 145−50.

(2) (a) Bannister, A. J.; Kouzarides, T. *Cell Res.* **2011**, *21* (3), 381−395. (b) Garcia-Ramirez, M.; Dong, F.; Ausio, J. *J. Biol. Chem.* **1992**, *267* (27), 19587−19595. (c) Shogren-Knaak, M.; Ishii, H.; Sun, J. M.; Pazin, M. J.; Davie, J. R.; Peterson, C. L. *Science* **2006**, *311* (5762), 844−847. (d) Robinson, P. J. J.; An, W.; Routh, A.; Martino, F.; Chapman, L.; Roeder, R. G.; Rhodes, D. *J. Mol. Biol.* **2008**, *381* (4), 816−825.

(3) Wolffe, A. P.; Hayes, J. J. *Nucleic Acids Res.* **1999**, *27* (3), 711−720.

(4) Allis, C. D. *Abstr Pap Am. Chem. S* **2002**, *224*, U45−U45.

(5) Luger, K.; Richmond, T. J. *Curr. Opin. Genet. Dev.* **1998**, *8* (2), 140−146.

(6) (a) Gao, M.; Nadaud, P. S.; Bernier, M. W.; North, J. A.; Hammel, P. C.; Poirier, M. G.; Jaroniec, C. P. *J. Am. Chem. Soc.* **2013**, *135* (41), 15278−15281. (b) Kato, H.; Gruschus, J.; Ghirlando, R.; Tjandra, N.; Bai, Y. W. *J. Am. Chem. Soc.* **2009**, *131* (42), 15104.

(7) Wang, X.; Moore, S. C.; Laszckzak, M.; Ausio, J. *J. Biol. Chem.* **2000**, *275* (45), 35013−20.

(8) Baneres, J. L.; Martin, A.; Parello, J. *J. Mol. Biol.* **1997**, *273* (3), 503−508.

(9) Zhou, B. R.; Feng, H.; Ghirlando, R.; Kato, H.; Gruschus, J.; Bai, Y. *J. Mol. Biol.* **2012**, *421* (1), 30−7.

(10) Allahverdi, A.; Yang, R.; Korolev, N.; Fan, Y.; Davey, C. A.; Liu, C.-F.; Nordenskiöld, L. *Nucleic Acids Res.* **2011**, *39*, 1680.

(11) Bang, E.; Lee, C. H.; Yoon, J. B.; Lee, D. W.; Lee, W. *J. Pept. Res.* **2001**, *58* (5), 389−98.

(12) (a) Levitt, M.; Warshel, A. *Nature* **1975**, *253* (5494), 694−8. (b) Su, C. C.; Long, F.; Zimmermann, M. T.; Rajashankar, K. R.; Jernigan, R. L.; Yu, E. W. *Nature* **2011**, *470* (7335), 558−62. (c) Whitford, P. C.; Ahmed, A.; Yu, Y.; Hennelly, S. P.; Tama, F.; Spahn, C. M.; Onuchic, J. N.; Sanbonmatsu, K. Y. *Proc. Natl. Acad. Sci. U. S. A.* **2011**, *108* (47), 18943−8. (d) Liao, T.; Zhang, Y.; Kekenes-Huskey, P. M.; Cheng, Y.; Michailova, A.; McCulloch, A. D.; Holst, M.; McCammon, J. A. Multi-core CPU or GPU-accelerated Multiscale Modeling for Biomolecular Complexes. *Mol. Based Math. Biol.* **2013**, *1*.10.2478/mlbmb-2013-0009 (e) Zhao, G.; Perilla, J. R.; Yufenyuy, E. L.; Meng, X.; Chen, B.; Ning, J.; Ahn, J.; Gronenborn, A. M.; Schulten, K.; Aiken, C.; Zhang, P. *Nature* **2013**, *497* (7451), 643−6.

(13) (a) Potoyan, D. A.; Papoian, G. A. *Proc. Natl. Acad. Sci. U. S. A.* **2012**, *109* (44), 17857−62. (b) Potoyan, D. A.; Papoian, G. A. *J. Am. Chem. Soc.* **2011**, *133* (19), 7405−7415.

(14) Korolev, N.; Yu, H.; Lyubartsev, A. P.; Nordenskiold, L. *Biopolymers* **2014**, *101*, 1051.

(15) (a) Bishop, T. C. *J. Biomol. Struct. Dyn.* **2005**, *22* (6), 673−685. (b) Biswas, M.; Voltz, K.; Smith, J. C.; Langowski, J. Role of Histone Tails in Structural Stability of the Nucleosome. *PLoS Comput. Biol.* **2011**, *7* (12), e1002279 10.1371/journal.pcbi.1002279 (c) Ettig, R.; Kepper, N.; Stehr, R.; Wedemann, G.; Rippe, K. *Biophys. J.* **2011**, *101* (8), 1999−2008. (d) Materese, C. K.; Savelyev, A.; Papoian, G. A. *J. Am. Chem. Soc.* **2009**, *131* (41), 15005−13. (e) Portella, G.; Battistini, F.; Orozco, M. *PLoS Comput. Biol.* **2013**, *9* (11), e1003354. (f) Biswas, M.; Langowski, J.; Bishop, T. C. *Wires Comput. Mol. Sci.* **2013**, *3* (4), 378−392.

(16) (a) Liu, H.; Duan, Y. *Biophys. J.* **2008**, *94* (12), 4579−85. (b) Yang, D.; Arya, G. *Phys. Chem. Chem. Phys.* **2011**, *13* (7), 2911−21.

(17) (a) Arya, G.; Schlick, T. *Proc. Natl. Acad. Sci. U. S. A.* **2006**, *103* (44), 16236−41. (b) Arya, G.; Schlick, T. *J. Phys. Chem. A* **2009**, *113* (16), 4045−59. (c) Perisic, O.; Collepardo-Guevara, R.; Schlick, T. *J. Mol. Biol.* **2010**, *403* (5), 777−802. (d) Kulaeva, O. I.; Zheng, G.; Polikanov, Y. S.; Colasanti, A. V.; Clauvelin, N.; Mukhopadhyay, S.; Sengupta, A. M.; Studitsky, V. M.; Olson, W. K. *J. Biol. Chem.* **2012**, *287* (24), 20248−57. (e) Collepardo-Guevara, R.; Schlick, T. *Proc. Natl. Acad. Sci. U. S. A.* **2014**, *111* (22), 8061−8066.

(18) Turner, B. M. *BioEssays* **2000**, *22* (9), 836−845.

(19) Ozer, G.; Luque, A.; Schlick, T. *Curr. Opin. Struct. Biol.* **2015**, *31*, 124.

(20) Hess, B.; Kutzner, C.; van der Spoel, D.; Lindahl, E. *J. Chem. Theory Comput.* **2008**, *4* (3), 435−447.

(21) Darden, T.; York, D.; Pedersen, L. *J. Chem. Phys.* **1993**, *98*, 10089−10092.

(22) Miyamoto, S.; Kollman, P. A. *J. Comput. Chem.* **1992**, *13*, 952−962.

(23) Feenstra, K. A.; Hess, B.; Berendsen, H. J. C. *J. Comput. Chem.* **1999**, *20*, 786−798.

(24) Bussi, G.; Donadio, D.; Parrinello, M. *J. Chem. Phys.* **2007**, *126* (1), 014101.

(25) Berendsen, H. J. C.; Postma, J. P. M.; DiNola, A.; Haak, J. R. *J. Chem. Phys.* **1984**, *81*, 3684−3690.

(26) Best, R. B.; Hummer, G. *J. Phys. Chem. B* **2009**, *113* (26), 9004−15.

(27) Hornak, V.; Abel, R.; Okur, A.; Strockbine, B.; Roitberg, A.; Simmerling, C. *Proteins: Struct., Funct., Genet.* **2006**, *65* (3), 712−25.

(28) Best, R. B.; Zhu, X.; Shim, J.; Lopes, P. E.; Mittal, J.; Feig, M.; Mackerell, A. D., Jr. *J. Chem. Theory Comput.* **2012**, *8* (9), 3257−3273.

(29) Papamokos, G. V.; Tziatzos, G.; Papageorgiou, D. G.; Georgatos, S. D.; Politou, A. S.; Kaxiras, E. *Biophys. J.* **2012**, *102* (8), 1926−33.

(30) Grauffel, C.; Stote, R. H.; Dejaegere, A. *J. Comput. Chem.* **2010**, *31* (13), 2434−51.

(31) Perez, A.; Marchan, I.; Svozil, D.; Sponer, J.; Cheatham, T. E., 3rd; Laughton, C. A.; Orozco, M. *Biophys. J.* **2007**, *92* (11), 3817−3829.

(32) Jorgensen, W. L.; Chandrasekhar, J.; Madura, J. D.; Impey, R. W.; Klein, M. L. *J. Chem. Phys.* **1983**, *79* (2), 926−935.

(33) Smith, D. E.; Dang, L. X. *J. Chem. Phys.* **1994**, *100* (5), 3757−3766.

(34) Humphrey, W.; Dalke, A.; Schulten, K. *J. Mol. Graphics* **1996**, *14* (1), 33−8 27−8..

(35) Bateman, A.; Martin, M. J.; O'Donovan, C.; Magrane, M.; Apweiler, R.; Alpi, E.; Antunes, R.; Ar-Ganiska, J.; Bely, B.; Bingley, M.; Bonilla, C.; Britto, R.; Bursteinas, B.; Chavali, G.; Cibrian-Uhalte, E.; Da Silva, A.; De Giorgi, M.; Dogan, T.; Fazzini, F.; Gane, P.; Castro, L. G.; Garmiri, P.; Hatton-Ellis, E.; Hieta, R.; Huntley, R.; Legge, D.; Liu, W. D.; Luo, J.; MacDougall, A.; Mutowo, P.; Nightin-Gale, A.; Orchard, S.; Pichler, K.; Poggioli, D.; Pundir, S.; Pureza, L.; Qi, G. Y.; Rosanoff, S.; Saidi, R.; Sawford, T.; Shypitsyna, A.; Turner, E.; Volynkin, V.; Wardell, T.; Watkins, X.; Watkins; Cowley, A.; Figueira, L.; Li, W. Z.; McWilliam, H.; Lopez, R.; Xenarios, I.; Bougueleret, L.; Bridge, A.; Poux, S.; Redaschi, N.; Aimo, L.; Argoud-Puy, G.; Auchincloss, A.; Axelsen, K.; Bansal, P.; Baratin, D.; Blatter, M. C.; Boeckmann, B.; Bolleman, J.; Boutet, E.; Breuza, L.; Casal-Casas, C.; De Castro, E.; Coudert, E.; Cuche, B.; Doche, M.; Dornevil, D.; Duvaud, S.; Estreicher, A.; Famiglietti, L.; Feuermann, M.; Gasteiger, E.; Gehant, S.; Gerritsen, V.; Gos, A.; Gruaz-Gumowski, N.; Hinz, U.; Hulo, C.; Jungo, F.; Keller, G.; Lara, V.; Lemercier, P.; Lieberherr, D.; Lombardot, T.; Martin, X.; Masson, P.; Morgat, A.; Neto, T.; Nouspikel, N.; Paesano, S.; Pedruzzi, I.; Pilbout, S.; Pozzato, M.; Pruess, M.; Rivoire, C.; Roechert, B.; Schneider, M.; Sigrist, C.; Sonesson, K.; Staehli, S.; Stutz, A.; Sundaram, S.; Tognolli, M.; Verbregue, L.; Veuthey, A. L.; Wu, C. H.; Arighi, C. N.; Arminski, L.; Chen, C. M.; Chen, Y. X.; Garavelli, J. S.; Huang, H. Z.; Laiho, K. T.; McGarvey, P.; Natale, D. A.; Suzek, B. E.; Vinayaka, C. R.; Wang, Q. H.; Wang, Y. Q.; Yeh, L. S.; Yerramalla, M. S.; Zhang, J. *Nucleic Acids Res.* **2015**, *43* (D1), D204−D212.

(36) Frishman, D.; Argos, P. *Proteins: Struct., Funct., Genet.* **1995**, *23* (4), 566−579.

(37) Ramachandran, G. N.; Ramakrishnan, C.; Sasisekharan, V. *J. Mol. Biol.* **1963**, *7* (1), 95−99.

(38) Patriksson, A.; van der Spoel, D. *Phys. Chem. Chem. Phys.* **2008**, *10* (15), 2073−2077.

(39) Davey, C. A.; Sargent, D. F.; Luger, K.; Maeder, A. W.; Richmond, T. J. *J. Mol. Biol.* **2002**, *319* (5), 1097−113.

DOI: 10.1021/jacs.5b04086
J. Am. Chem. Soc. 2015, 137, 10205−10215

(40) Schalch, T.; Duda, S.; Sargent, D. F.; Richmond, R. K. *Nature* **2005**, *436*, 138−141.
(41) Camilloni, C.; Cavalli, A.; Vendruscolo, M. *J. Phys. Chem. B* **2013**, *117* (6), 1838−1843.
(42) Camilloni, C.; De Simone, A.; Vranken, W. F.; Vendruscolo, M. *Biochemistry* **2012**, *51* (11), 2224−31.
(43) Kohlhoff, K. J.; Robustelli, P.; Cavalli, A.; Salvatella, X.; Vendruscolo, M. *J. Am. Chem. Soc.* **2009**, *131* (39), 13894−5.
(44) Tribello, G. A.; Bonomi, M.; Branduardi, D.; Camilloni, C.; Bussi, G. *Comput. Phys. Commun.* **2014**, *185* (2), 604−613.
(45) Laio, A.; Parrinello, M. *Proc. Natl. Acad. Sci. U. S. A.* **2002**, *99* (20), 12562−12566.
(46) Atkins, P. W.; De Paula, J. *Atkins' Physical chemistry*, 9th ed.; Oxford University Press: Oxford, 2010; p 972.
(47) (a) Zhang, Q.; Beard, D. A.; Schlick, T. *J. Comput. Chem.* **2003**, *24* (16), 2063−74. (b) Arya, G.; Zhang, Q.; Schlick, T. *Biophys. J.* **2006**, *91* (1), 133−50. (c) Beard, D. A.; Schlick, T. *Structure* **2001**, *9* (2), 105−14. (d) Beard, D. A.; Schlick, T. *Biopolymers* **2001**, *58* (1), 106−115. (e) Collepardo-Guevara, R.; Schlick, T. *Biophys. J.* **2011**, *101* (7), 1670−80. (f) Collepardo-Guevara, R.; Schlick, T. *Nucleic Acids Res.* **2012**, *40* (18), 8803−17. (g) Sun, J.; Zhang, Q.; Schlick, T. *Proc. Natl. Acad. Sci. U. S. A.* **2005**, *102* (23), 8180−5. (h) Luque, A.; Collepardo-Guevara, R.; Grigoryev, S.; Schlick, T. *Nucleic Acids Res.* **2014**, *42*, 7553.
(48) Jian, H.; Vologodskii, A.; Schlick, T. *J. Comput. Phys.* **1997**, *136*, 168−179.
(49) Schuler, B.; Lipman, E. A.; Steinbach, P. J.; Kumke, M.; Eaton, W. A. *Proc. Natl. Acad. Sci. U. S. A.* **2005**, *102* (8), 2754−2759.
(50) Lu, Y. J.; Weers, B.; Stellwagen, N. C. *Biopolymers* **2002**, *61* (4), 261−275.
(51) Lavelle, C.; Victor, J. M.; Zlatanova, J. *Int. J. Mol. Sci.* **2010**, *11* (4), 1557−79.
(52) De Simone, A.; Cavalli, A.; Hsu, S. T.; Vranken, W.; Vendruscolo, M. *J. Am. Chem. Soc.* **2009**, *131* (45), 16332−3.
(53) Wang, X. D.; Hayes, J. J. *Mol. Cell. Biol.* **2008**, *28* (1), 227−236.
(54) Garciaramirez, M.; Rocchini, C.; Ausio, J. *J. Biol. Chem.* **1995**, *270* (30), 17923−17928.
(55) Thomas, J. O.; Furber, V. *FEBS Lett.* **1976**, *66* (2), 274−280.
(56) Smith, C. M.; Gafken, P. R.; Zhang, Z. L.; Gottschling, D. E.; Smith, J. B.; Smith, D. L. *Anal. Biochem.* **2003**, *316* (1), 23−33.
(57) Braunstein, M.; Sobel, R. E.; Allis, C. D.; Turner, B. M.; Broach, J. R. *Mol. Cell. Biol.* **1996**, *16* (8), 4349−4356.
(58) (a) Luebben, W. R.; Sharma, N.; Nyborg, J. K. *Proc. Natl. Acad. Sci. U. S. A.* **2010**, *107* (45), 19254−9. (b) Schiltz, R. L.; Mizzen, C. A.; Vassilev, A.; Cook, R. G.; Allis, C. D.; Nakatani, Y. *J. Biol. Chem.* **1999**, *274* (3), 1189−92.
(59) FarzadFard, F.; Gharaei, N.; Pezeshk, H.; Marashi, S. A. *J. Struct. Biol.* **2008**, *161* (1), 101−110.
(60) Song, F.; Chen, P.; Sun, D.; Wang, M.; Dong, L.; Liang, D. *Science* **2014**, *344*, 376−380.
(61) Schlick, T.; Hayes, J.; Grigoryev, S. *J. Biol. Chem.* **2012**, *287* (8), 5183−91.
(62) (a) Maeshima, K.; Imai, R.; Tamura, S.; Nozaki, T. *Chromosoma* **2014**, *123* (3), 225−37. (b) Ozer, G.; Luque, A.; Schlick, T. *Curr. Opin. Struct. Biol.* **2014**, *31*, 124.
(63) (a) Routh, A.; Sandin, S.; Rhodes, D. *Proc. Natl. Acad. Sci. U. S. A.* **2008**, *105* (26), 8872−8877. (b) Correll, S. J.; Schubert, M. H.; Grigoryev, S. A. *EMBO J.* **2012**, *31* (10), 2416−26.
(64) Sun, F. L.; Cuaycong, M. H.; Elgin, S. C. R. *Mol. Cell. Biol.* **2001**, *21* (8), 2867−2879.
(65) Akhtar, A.; Becker, P. B. *Mol. Cell* **2000**, *5* (2), 367−375.
(66) Dorigo, B.; Schalch, T.; Bystricky, K.; Richmond, T. J. *J. Mol. Biol.* **2003**, *327* (1), 85−96.
(67) Hong, L.; Schroth, G. P.; Matthews, H. R.; Yau, P.; Bradbury, E. M. *J. Biol. Chem.* **1993**, *268* (1), 305−314.

DOI: 10.1021/jacs.5b04086
J. Am. Chem. Soc. 2015, 137, 10205−10215